Applied Catalysis B: Environmental 97 (2010) 381–388

Contents lists available at ScienceDirect

Applied Catalysis B: Environmental

journal homepage: www.elsevier.com/locate/apcatb

Time-resolved *operando* X-ray absorption study of $CuO–CeO_2/Al_2O_3$ catalyst during total oxidation of propane

Konstantinos Alexopoulos[a], Mettu Anilkumar[a], Marie-Françoise Reyniers[a,*], Hilde Poelman[a], Sylvain Cristol[c], Veerle Balcaen[a], Philippe M. Heynderickx[a], Dirk Poelman[b], Guy B. Marin[a]

[a] *Laboratory for Chemical Technology, Ghent University, Krigslaan 281, S5, B-9000, Ghent, Belgium*
[b] *Department of Solid State Science, Ghent University, Krigslaan 281, S1, B-9000, Ghent, Belgium*
[c] *Unité de Catalyse et Chimie du Solide (UCCS) UMR CNRS 8181, Université de Lille 1, Cité scientifique (Bâtiment C3), F-59655 Villeneuve d'Ascq, France*

ARTICLE INFO

Article history:
Received 22 February 2010
Received in revised form 9 April 2010
Accepted 17 April 2010
Available online 24 April 2010

Keywords:
Structure–activity investigation
Supported metal oxides
Reduction and oxidation mechanism
Propane total oxidation
Volatile organic compounds

ABSTRACT

The local structure of the copper phase of a $CuO–CeO_2/Al_2O_3$ catalyst and its activity for the total oxidation of propane have been studied under working conditions, using time-resolved X-ray absorption spectroscopy (XAS) in transmission mode at the Cu K edge coupled with on-line mass spectrometry (MS). In the temperature range of 573–723 K, the copper phase of the catalyst remains oxidized (i.e. Cu^{2+}) during total oxidation reaction conditions ($1\%C_3H_8–5\%O_2$/He), while three species are present (i.e. Cu^{2+}, Cu^{1+} and Cu^0) during reduction ($2\%C_3H_8$/He) and re-oxidation ($10\%O_2$/He) treatments where a two-step mechanism is found. Catalyst reduction is fully reversible, as the Cu^{2+} nature of the catalyst is recovered after a reduction–oxidation cycle. Re-oxidation of the catalyst is two orders of magnitude faster than its reduction and has an apparent activation energy of 24 kJ/mol. On the other hand, catalyst reduction requires an apparent activation energy of 70 kJ/mol, which is equal to the apparent activation energy determined under total oxidation reaction conditions. These results give support to a Mars–van-Krevelen reaction scheme with the copper phase of the catalyst being close to a fully oxidized state.

1. Introduction

The emission of volatile organic compounds (VOCs) is considered to be an important contributor to air pollution. In recent years protection of the environment has received considerable attention, as quality of life is strongly connected to a clean environment. Catalytic oxidation is one of the most effective techniques used for the elimination of VOCs. Propane can be considered a model VOC, since it is a typical industrial flue gas and is also emitted in considerable amounts by liquid petroleum gas powered vehicles [1,2]. Typically, the most effective catalysts that have been used for the total oxidation of organic compounds are supported noble metal catalysts (Pt, Pd, Rh, etc.) [3,4]. Although the supported noble metal catalysts are very active, they are very expensive and unstable at reaction conditions. Supported metal (Fe, Cu, Cr, Mn, Co, etc.) oxides are widely used as alternative oxidation catalysts, due to their availability and their high surface area [5,6]. In particular, $CuO–CeO_2/Al_2O_3$ catalysts are reported to be efficient and environmentally benign for emission control reactions, steam reforming of methanol, and water gas shift reactions [7–11]. According to Larsson and Andersson [12,13], the addition of CeO_2 to CuO/Al_2O_3 catalysts results in a substantial increase of activity for CO combustion as well as for total oxidation of both ethyl acetate and ethanol. The same authors reported that CeO_2 enhances the dispersion of the active phase of supported catalysts and improves the thermal resistance of the alumina support. Fernández-García et al. [14] also suggested that ceria reduces the particle size of the CuO phase in a $CuO–CeO_2/Al_2O_3$ catalyst as compared to a CuO/Al_2O_3 catalyst. Moreover, as evidenced by temperature programmed reduction (TPR) measurements, the presence of Ce in the $CuO–CeO_2/Al_2O_3$ catalyst results in an enhancement of the reducibility of the active copper phase [15]. Interestingly enough, electrochemical studies attributed the promoting effect of Ce to the lower redox potentials of Cu in $CuO–CeO_2$ as compared to those in CuO and $CuO–ZrO_2$ [16].

The aim of this work is to investigate the structure and oxidation state of the catalyst's active copper phase under total oxidation reaction conditions by *operando* time-resolved X-ray absorption spectroscopy (XAS) coupled with mass spectrometry (MS). These *in situ* measurements can also help to understand the complex reaction mechanism and to observe possible transient species. As catalytic changes can occur rather fast under working conditions, time resolution together with data quality are key parameters to follow accurately the dynamic behavior of the catalytic system. To this end, energy dispersive XAS and MS measurements are combined, allowing simultaneous time-resolved structural analysis of

* Corresponding author. Tel.: +32 92645677; fax: +32 92645824.
E-mail address: MarieFrancoise.Reyniers@ugent.be (M.-F. Reyniers).

0926-3373/$ – see front matter © 2010 Elsevier B.V. All rights reserved.
doi:10.1016/j.apcatb.2010.04.022

Table 1
Characterization results of as received $CuO–CeO_2/Al_2O_3$ catalyst [17].

BET surface area (m^2/g)	156		
Composition	Al	Cu	Ce
ICP (wt%)	38.75	9.25	5.2
EDX (at%)	36.4	4	0.8
XPS (at%)	38	2.5	0.1
XRD crystal size (nm)			
CuO	~100		
CeO_2	6		
Al_2O_3	4		

the catalyst and kinetic analysis of the reaction within sub-second time resolution.

Recently, Silversmit et al. [17] investigated the changes in the local structure of Cu and Ce in a $CuO–CeO_2/Al_2O_3$ catalyst under propane reduction and oxidation conditions using XAS measurements on a minute time scale. It was reported that, under propane exposure at reaction temperatures of 600–763 K, Cu^{2+} is reduced to metallic Cu^0 in a two-step reduction process with Cu^{1+} appearing as a transient phase. In addition, Ce^{4+} is found to reduce partially to Ce^{3+} during temperature programmed reduction (TPR) with propane, reaching a Ce^{4+} conversion of about 32% at 763 K. However, no intermediate re-oxidation spectra could be recorded because of the limited time resolution of the XAS measurements and no on-line gas analysis was reported in that study. In contrast, the present study focuses on the structural changes of the catalyst during both reduction and re-oxidation with simultaneous analysis of the reactor effluent using XAS/MS measurements on a sub-second time scale. By acquiring these measurements simultaneously, a structure–activity relationship for the catalyst can be derived. In addition, an attempt has been made in this study to obtain insight into the reaction mechanism by comparing the results obtained from the solid state and the gas phase analysis. Finally, a quantitative comparison between ab initio XANES (X-ray absorption near-edge structure) calculations and experimental spectra has shown to provide valuable information for the structure of the catalyst.

2. Experimental and theoretical methods

2.1. Catalyst

$CuO–CeO_2/Al_2O_3$ was prepared by impregnating γ-Al_2O_3 with $Cu(NO_3)_2$ and $Ce(NO_3)_4$ precursors, followed by drying and calcination above 723 K. The characteristics of the catalyst are presented in Table 1. XRD gives no indication of bulk copper aluminates being formed, which is in accordance with the low calcination temperature, while the diffraction peaks found for CuO show that the catalyst consists mainly of large CuO aggregates (~100 nm) [17].

2.2. Operando XANES/MS measurements

Time-resolved *operando* XAS/MS experiments on the $CuO–CeO_2/Al_2O_3$ catalyst were performed at the energy dispersive beamline ID24 of ESRF. The average energy and current in the storage ring during all measurements were 6 GeV and 75 mA, respectively. A bent polychromator crystal Si [3 1 1] was utilized to focus and disperse a polychromatic X-ray beam onto the sample. In this configuration the beam passes through the sample and then diverges towards a position-sensitive detector, where beam position is correlated to energy. Copper K-edge X-ray absorption spectra were measured in transmission mode with a 16 bit FReLoN (fast readout low noise) solid-state detector [18]. The incident intensity, I_0, was measured through air before measuring the intensity, I_t, transmitted by the sample. A spectrum of a Cu metal foil was recorded after each refill of the storage ring (i.e. every 8 h), in order to calibrate the energy scale of the detector.

The experiments were carried out in an *operando* cell designed to resemble the operation of a reactor under plug flow conditions [19]. The reactor of this experimental cell consists of a quartz capillary tube mounted horizontally in the setup. The undiluted grounded catalyst (75–100 μm) was loaded between two glass wool plugs in the quartz capillary with an inner diameter of 0.9 mm and an outer diameter of 1 mm (Hilgenberg GmbH). The flow sheet of the experimental setup is given in Fig. 1.

Prior to the start of the reaction experiments, the catalyst was pretreated at 423 K under oxygen flow (10% O_2/He with total flow rate of 1.5×10^{-5} mol/s) for one hour. The experiment consisted of imposing step pulses on the catalytic system using fast switching valves. The isothermal step-response experiments involved catalyst reduction with propane (2% C_3H_8/He) and catalyst oxidation with oxygen (10% O_2/He), followed by total oxidation reaction under simultaneous flow of propane and oxygen (1% C_3H_8–5% O_2/He). These experiments were performed at four different temperatures (573, 623, 673 and 723 K) under atmospheric pressure. During the catalyst reduction/oxidation cycles a constant total flow rate was used (i.e. 1.5×10^{-5} mol/s), while under total oxidation reaction conditions a range of space times (38.3–127.7 kg s/mol) was obtained by varying the total flow rate (i.e. 0.5–1.5×10^{-5} mol/s). During these step-response experiments, energy dispersive Cu K XANES of the catalyst were recorded at the inlet of the reactor with a time resolution of 0.1 s, while on-line MS measurements at the outlet of the reactor were carried out with the same time resolution. As the X-ray beam is a tight focused one, the energy dispersive XANES is a spatially resolved and element specific probe as compared to the mass spectrometer that integrates over the complete catalyst bed [20]. The following amu's were continuously registered: 4, 12, 14, 18, 28, 29, 32, 41, and 44. To obtain quantitative results from the MS gas phase analysis, i.e. gas phase compositions in mol%, calibration of the MS was performed with known mixtures of non overlapping gas components and the analysis procedure of the MS-software (Quadstar™) was followed. For the XANES analysis, as the raw data were in pixels of the camera, energy calibration was done by comparing a Cu foil measured in pixels to one measured in eV. Determination of the edge position, background subtraction and normalization of the calibrated raw XANES data was done with Athena [21]. Moreover, a principal component analysis (PCA) followed by a linear combination fit (LCF) was applied for the region around the edge (−20 eV to 30 eV) to quantify the atomic ratio of $Cu^{2+}/Cu^{1+}/Cu^0$ in the active phase, using as standard for Cu^{2+} the spectrum of the fully oxidized catalyst sample (before treatment with propane), for Cu^0 the spectrum of the fully reduced catalyst sample (after treatment with propane), and for Cu^{1+} the spectrum of a Cu_2O reference [17,22,23].

2.3. Ab initio XANES calculations

Theoretical calculations of XANES were performed using the FDMNES package [24] within the muffin-tin approximation. A Lorentzian energy-dependent convolution was applied to the calculated spectrum, in order to account for several broadening effects not included in the theory. The structure of the active phase was verified before and after the treatment of the catalyst with propane using cluster models (with a radius of 830 pm) based on the monoclinic CuO structure and on the fcc Cu structure, respectively. Theoretical spectra calculated with these models for a range of interatomic distances were compared with experimental spectra and refined bond distances between neighboring atoms were obtained from the best fit between theory and experiment.

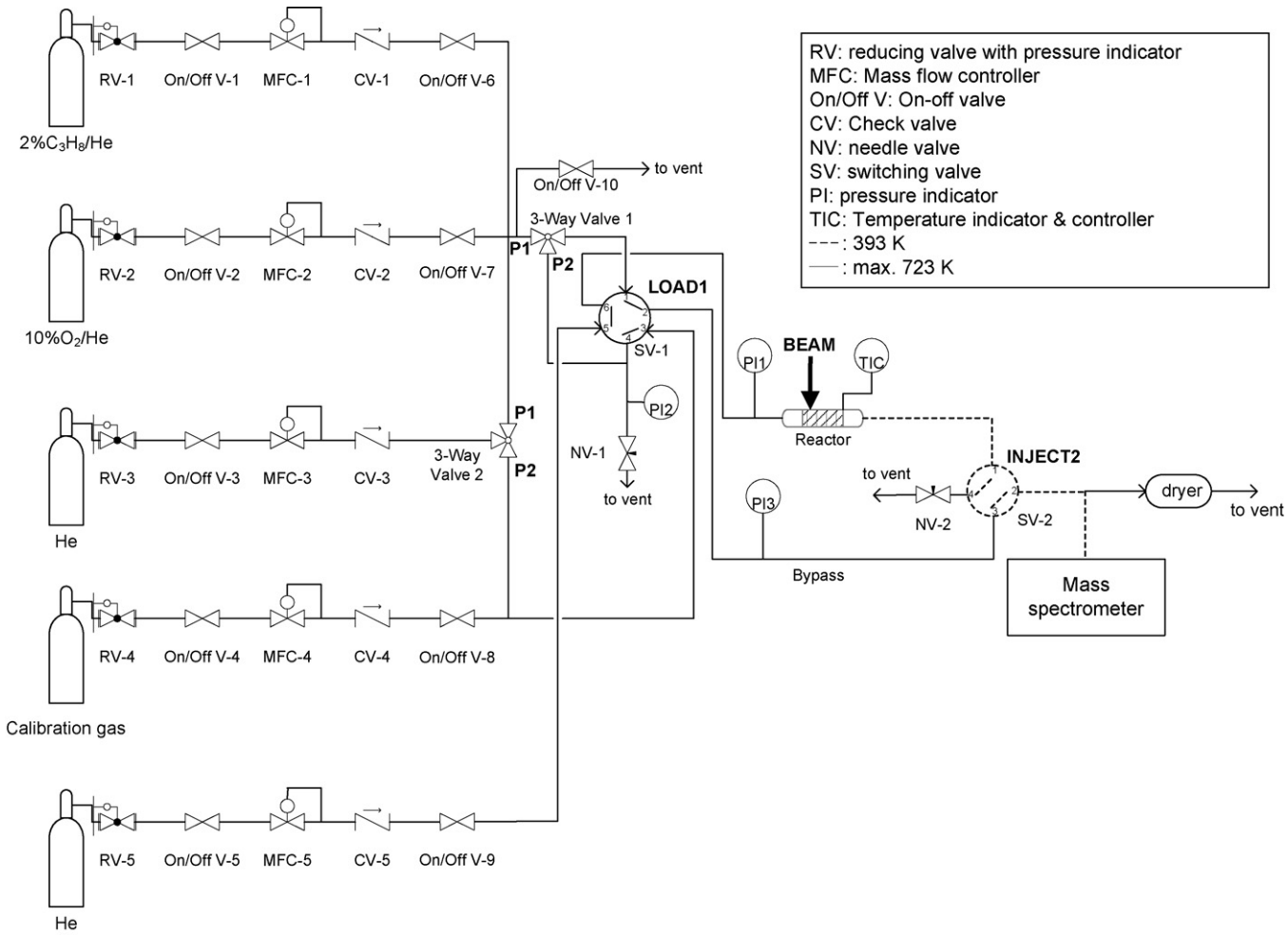

Fig. 1. Flow diagram of the experiment.

3. Results and discussion

3.1. Structure of the CuO–CeO_2/Al_2O_3 catalyst at ambient and pretreatment conditions

Fig. 2 presents Cu K XANES spectra of reference samples, i.e. CuO, Cu_2O, Cu at ambient conditions together with the spectrum of the CuO–CeO_2/Al_2O_3 catalyst. Clearly, the spectrum of CuO–CeO_2/Al_2O_3 closely resembles that of CuO, exhibiting a weak pre-edge feature at 8978 eV, corresponding to a dipole-forbidden 1s → 3d electronic transition, a shoulder feature at 8986 eV, attributed to a 1s → $4p_{xy}$ electronic transition, and a white line at 8998 eV [25]. Thus, Cu^{2+} species are present in the catalyst as prepared. In addition, Cu K XANES spectra of the CuO–CeO_2/Al_2O_3 catalyst recorded during heating in He and after pretreatment with oxygen (not shown) indicate no significant differences and suggest that the copper phase of the catalyst remains in its initial Cu^{2+} state under these conditions.

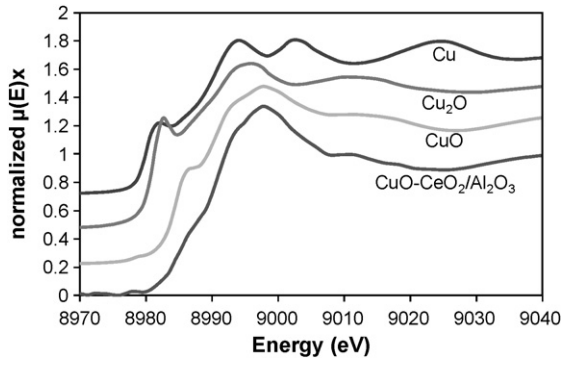

Fig. 2. Cu K XANES of Cu foil, Cu_2O, CuO and CuO–CeO_2/Al_2O_3 catalyst at ambient conditions.

3.2. Structure and activity of the CuO–CeO_2/Al_2O_3 catalyst during reduction with propane

The evolution of the Cu K XANES spectra of the CuO–CeO_2/Al_2O_3 catalyst under reduction with propane at 723 K is presented in Fig. 3, where time zero corresponds to the time when the switch in the reactor feed was made from inert He to 2%C_3H_8/He. Significant changes can be seen clearly in the resulting spectra. During the reduction of the catalyst, the white line's intensity decreases while the shoulder feature at the edge shifts to lower energies and the weak pre-edge peak at 8978 eV, attributed to Cu^{2+} species, disappears. At the shoulder feature, the development of a peak is evident. However, after about 1 min this peak starts to disappear, as illustrated in the inset of Fig. 3, where the two trends can be seen. This phenomenon is not expected to occur if only two components are present during reduction and, therefore, is a clear indication of the presence of an intermediate phase. This well-defined peak around 8984 eV is characteristic of the 1s–$4p_{xy}$ transition attributed to Cu^{1+} species found in Cu_2O (see Fig. 2) [26]. Towards the end of the reduc-

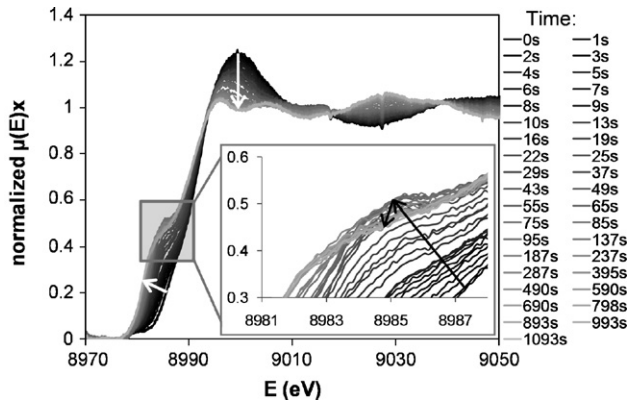

Fig. 3. Evolution of Cu K XANES spectra of CuO–CeO_2/Al_2O_3 catalyst during reduction with 2%C_3H_8/He at 723 K.

tion treatment, this peak ascribed to Cu^{1+} species disappears and the spectrum of the catalyst closely resembles that of a Cu foil (see Figs. 2 and 3), indicating that a full reduction of the copper phase is reached. Clearly, all observed changes in the Cu K XANES spectra of the catalyst can be well explained if a stepwise reduction from CuO to Cu_2O to Cu is assumed. Moreover, principal component analysis for catalyst reduction at 573, 623, 673 and 723 K identified three different species, which are attributed to Cu^{2+}, Cu^{1+} and Cu^0.

According to literature [27–33], CuO can be reduced either in a direct ($Cu^{2+} \rightarrow Cu^0$) or in a two-step process ($Cu^{2+} \rightarrow Cu^{1+} \rightarrow Cu^0$). CO-TPR investigation of the reducibility of copper species in the CuO/Al_2O_3 and CuO–CeO_2/Al_2O_3 catalysts has been reported by Martínez-Arias et al. [27]. This investigation revealed that both Cu^{1+} and Cu^0 species are formed by interaction of CO with the catalyst below 573 K. Cu K XANES result for a CuO/ZnO_2 catalyst showed a transient Cu_2O phase during H_2 reduction and oxidative methanol steam reforming [28,29]. Furthermore, Cu K XANES measurements of a CuO/ZrO_2 catalyst indicated the presence of three Cu species (i.e. CuO, Cu_2O and Cu) during reduction with C_3H_8 [30]. On the other hand, CuO supported on zeolites is directly reduced from CuO to metallic Cu without the occurrence of an intermediate monovalent Cu species [31]. An *in situ* Cu K XANES/H_2-TPR study of Cu-ZSM-5 showed that although three Cu species were evident during reduction, the signal for Cu^{1+} rapidly disappeared at higher Cu loadings [32]. Moreover, Kim et al. [33] found no Cu_2O as an intermediate during reduction of the unsupported CuO powder with 5% H_2/He (flow rate 15–20 cm^3/min) at 473 K, while the authors suggested that one has to limit the flow of hydrogen or use a steep temperature ramp in order to observe the formation of Cu_2O. Clearly, the reduction pathway depends on the amount of Cu present, the type of support used and the reduction conditions.

The evolution of the composition of the copper phase from the LCF analysis together with the corresponding gas phase analysis from the MS during reduction with propane at 723 K is presented in Fig. 4. As can be seen from Fig. 4, a transition from Cu^{2+} to Cu^0 occurs and the existence of a transient Cu^{1+} phase is observed. The maximum amount of Cu^{1+} is observed at $t = 40$ s and is about 40%. The MS data for the gas phase analysis shows an initial complete uptake of propane until $t = 15$ s and a maximum CO_2 concentration of about 2% at 20 s. At the end of the reduction treatment, both Cu^{2+} and the transient Cu^{1+} phase disappear and only the Cu metal phase is present in the LCF analysis. Meanwhile, the MS analysis shows a constant concentration of 2% for C_3H_8, while the CO_2 concentration drops to zero at the end of the measurement. Overall, these results indicate that CuO is reduced in a two-step process (i.e. $Cu^{2+} \rightarrow Cu^{1+} \rightarrow Cu^0$) by reaction with C_3H_8 and hereby producing CO_2. It is also worth noting that the solid phase analysis using XANES agrees well with the MS gas phase analysis, since no more

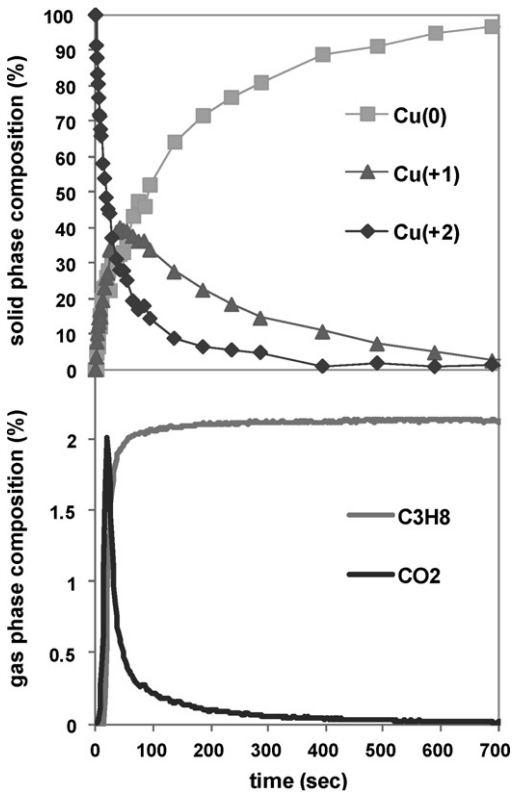

Fig. 4. Evolution of the composition of the active phase of the CuO–CeO_2/Al_2O_3 catalyst and of the gas phase at the reactor outlet during reduction with 2%C_3H_8/He at 723 K.

CO_2 is detected once the XANES measurements indicate that full reduction of the catalyst has been reached.

In Fig. 5a, the conversion of the Cu^{2+} species ($X_{Cu^{2+}}$), as determined from the LCF analysis, during reduction at all temperatures is presented. To obtain an estimate of the rate of reduction, characteristic time constants for catalyst reduction (τ_{red}) have been calculated assuming a first order approximation:

$$X_{Cu^{2+}} = 1 - e^{-t/\tau_{red}} \quad (1)$$

In order not to include oxygen diffusion on the estimated rate of surface reduction, only the initial regime as shown in Fig. 5a has been modeled using Eq. (1). The time constants for catalyst reduction are summarized in Table 2, where it can be seen that the process significantly speeds up at higher temperatures. Plotting the time constants in an Arrhenius diagram (Fig. 5b) allows determining an apparent activation energy of 70.0 kJ/mol for catalyst reduction.

3.3. Structure and activity of the CuO–CeO_2/Al_2O_3 catalyst during re-oxidation with dioxygen

To determine whether the reduced copper phase of the catalyst can be re-oxidized and to establish whether the transient Cu_2O phase is also observed during catalyst re-oxidation, isothermal step-response experiments were carried out by switching the

Table 2
Time constants for catalyst reduction and oxidation with 2%C_3H_8/He and 10%O_2/He, respectively.

T (K)	τ_{red} (s)	τ_{ox} (s)
573	431	1.1
623	149	1.0
673	44	0.5
723	22	0.4

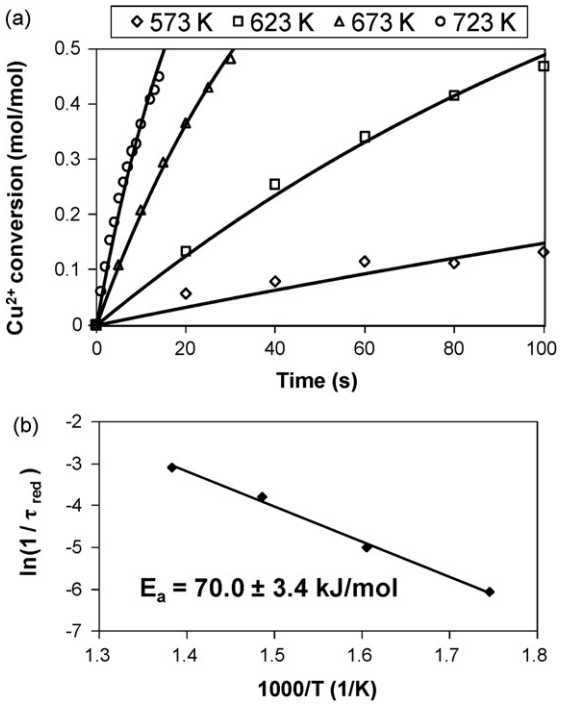

Fig. 5. (a) Conversion of Cu^{2+} species during reduction of the CuO–CeO_2/Al_2O_3 catalyst with 2%C_3H_8/He at different temperatures; full lines are calculated according to Eq. (1) with the time constants given in Table 2; (b) Arrhenius relation for catalyst reduction with 2%C_3H_8/He; activation energies are reported with their individual approximate 95% confidence intervals.

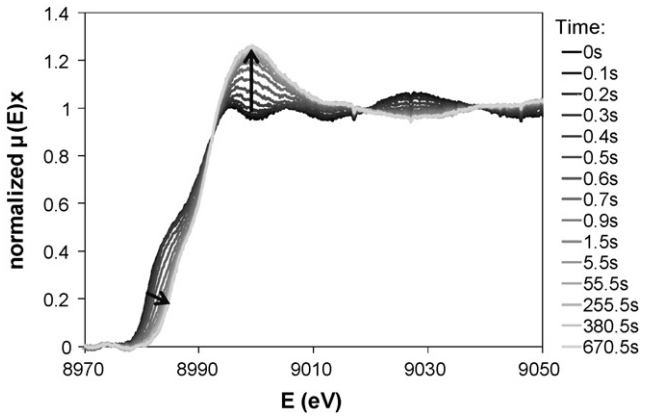

Fig. 6. Evolution of Cu K XANES spectra of CuO–CeO_2/Al_2O_3 catalyst during re-oxidation with 10%O_2/He at 723 K.

reactor feed from inert He to 10%O_2/He. The corresponding XANES results at 723 K reveal (see Fig. 6) that the changes in the spectra are consistent with a shift of the edge to higher energies and an increase of the white line intensity, indicating that the Cu^{2+} nature of the catalyst is recovered after a re-oxidation treatment. Similar to catalyst reduction, principal component analysis for catalyst re-oxidation at 573, 623, 673 and 723 K revealed three different species attributed to Cu^{2+}, Cu^{1+} and Cu^0.

The composition of the copper phase of the catalyst was determined using LCF and is presented in Fig. 7a as a function of time at 723 K. As seen from this figure, a transition from Cu^0 to Cu^{2+} occurs and the existence of an intermediate Cu^{1+} phase is observed. The maximum amount of Cu^{1+} is observed at $t = 0.5$ s and is about 20%. These results clearly suggest that the reduced catalyst can be re-oxidized reversibly and that catalyst re-oxidation proceeds via the same two-step mechanism as the one found for the catalyst reduction. This finding agrees well with previous studies of oxidation of pure metal Cu at 573 K with 5% O_2/He (flow rate 20 cm^3/min) [34]. In addition, by following the response of the oxygen using the MS, it was possible to measure the oxygen uptake from the catalyst during re-oxidation (see Fig. 7b). Taking into account the amount of oxygen contained in the CuO and CeO_2 phase of the catalyst, which is calculated from the ICP values assuming that Cu and Ce

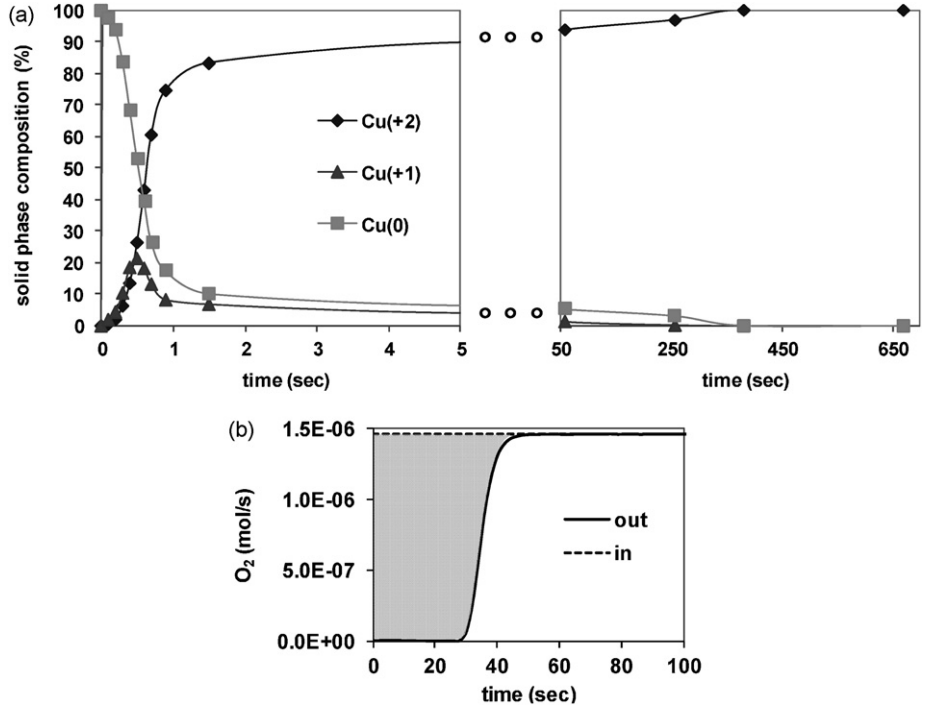

Fig. 7. (a) Evolution of the composition of the active phase of CuO–CeO_2/Al_2O_3 catalyst during re-oxidation with 10%O_2/He at 723 K; (b) molar flow rate of O_2 during catalyst re-oxidation at 723 K with shaded area corresponding to the oxygen uptake.

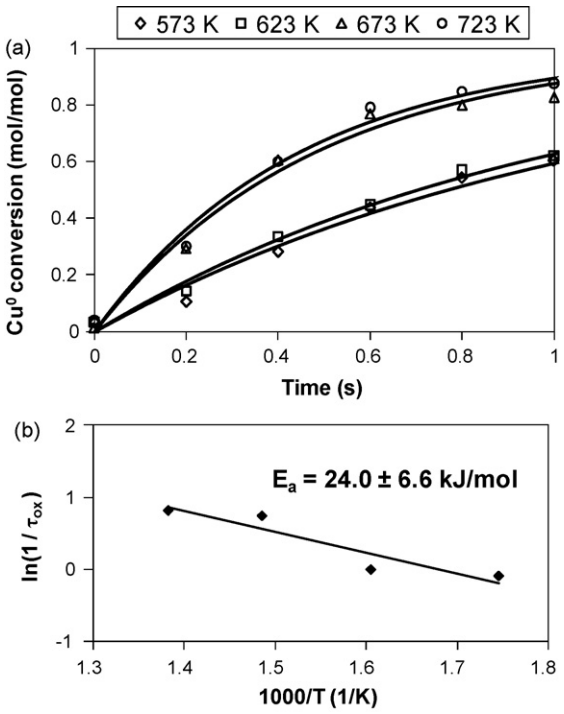

Fig. 8. (a) Conversion of Cu^0 species during re-oxidation of the $CuO–CeO_2/Al_2O_3$ catalyst with $10\%O_2$/He at different temperatures; full lines are calculated according to Eq. (2) with the time constants given in Table 2; (b) Arrhenius relation for catalyst oxidation with $10\%O_2$/He; activation energies are reported with their individual approximate 95% confidence intervals.

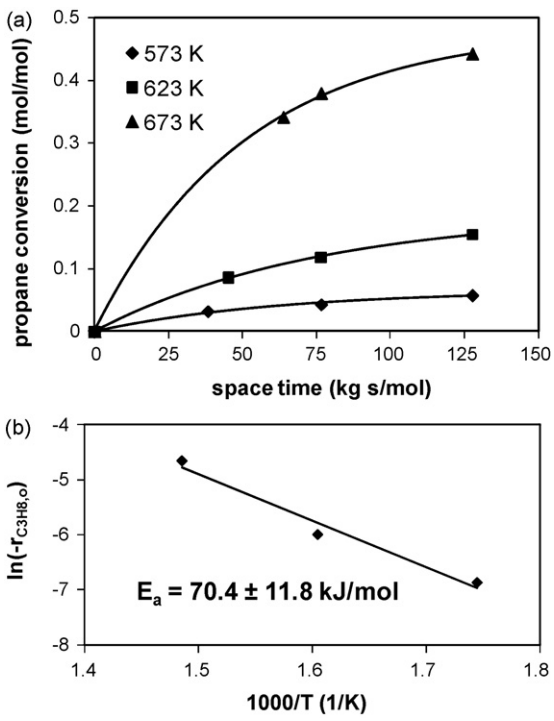

Fig. 9. (a) Propane conversion versus space time at different temperatures under total oxidation reaction conditions ($1\%C_3H_8–5\%O_2$/He); full lines are calculated according to Eq. (3) with the parameters given in Table 3; (b) initial reaction rate versus temperature under total oxidation reaction conditions ($1\%C_3H_8–5\%O_2$/He); activation energies are reported with their individual approximate 95% confidence intervals.

are completely oxidized [17], the oxygen consumed for the catalyst re-oxidation at 723 K can be explained by 100% reduction of CuO and 28% reduction of CeO_2. This result is in accordance with the oxygen consumption attributed to the total oxidation of propane during catalyst reduction (Fig. 4) and is in good agreement with the data reported by Silversmit et al. [17]. These authors reported for the same catalyst and temperature a 30% reduction of Ce^{4+} using Ce L_3 XANES analysis.

In Fig. 8a, the conversion of the Cu^0 species (X_{Cu^0}), as determined from the LCF analysis, during re-oxidation at all temperatures is presented. Similar as for reduction, characteristic time constants for catalyst re-oxidation (τ_{ox}) have been calculated, assuming a first order approximation:

$$X_{Cu^0} = 1 - e^{-t/\tau_{ox}} \quad (2)$$

In order not to include oxygen diffusion on the estimated rate of surface re-oxidation, only the initial regime as shown in Fig. 8a has been modeled using Eq. (2). The time constants for catalyst re-oxidation are summarized in Table 2, where they are compared with the time constants for catalyst reduction. Similar to reduction, catalyst re-oxidation speeds up with increasing temperature. The smallest time constant under reduction conditions is about 22 s at 723 K, while at the same temperature the time constant for re-oxidation is about 0.4 s. From the data in Table 2, it can be concluded that re-oxidation of the catalyst occurs much faster, i.e. some two orders of magnitude faster, than its reduction for all temperatures and this becomes more pronounced at lower temperatures. In accordance with this observation, plotting the time constants in an Arrhenius diagram (Fig. 8b) yields an apparent activation energy of 24.0 kJ/mol for catalyst oxidation, which is 46 kJ/mol lower than the apparent activation energy for catalyst reduction.

3.4. Structure and activity of the $CuO–CeO_2/Al_2O_3$ catalyst during total oxidation conditions

The effect of temperature on propane conversion at different space times over the $CuO–CeO_2/Al_2O_3$ catalyst is displayed in Fig. 9a. The propane conversion increases as a function of temperature at all space times. The maximum propane conversion of 45% is observed at 673 K at space time of 128 kg s/mol. The MS gas phase analysis at different temperatures yields CO_2 as the main product of propane oxidation. In order to estimate initial reaction rates, the following equation [35] is regressed to the experimental propane conversion ($X_{C_3H_8}$) vs. space time ($W_{cat}/F_{C_3H_8,0}$) data for each temperature:

$$X_{C_3H_8} = A(1 - e^{-B(W_{cat}/F_{C_3H_8,0})}) \quad (3)$$

From the initial slope of the propane conversion versus space time curves (i.e. first derivative of Eq. (3) at zero space time), initial reaction rates were calculated at different temperatures (Table 3). To determine the apparent activation energy under total oxidation conditions, these initial reaction rates are presented in an Arrhenius plot (see Fig. 9b). The apparent activation energy for propane total oxidation reaction is 70.4 kJ/mol.

It is important to note that the apparent activation energy under total oxidation reaction conditions as determined from the MS analysis is identical to the apparent activation energy under reduction

Table 3
Parameter estimates of Eq. (3) and initial reaction rates under total oxidation reaction conditions ($1\%C_3H_8–5\%O_2$/He).

T (K)	A (mol/mol)	B (mol kg^{-1} s^{-1})	$r_{C_3H_8,0} = A \cdot B$ (mol kg^{-1} s^{-1})
573	0.0657	0.0157	0.0010
623	0.1886	0.0131	0.0025
673	0.4823	0.0196	0.0095

Table 4
Bond distances obtained from the Cu K XANES fit for the oxidized and reduced catalyst and for the CuO and Cu references together with their respective crystallographic values.

Structure	Bond	Crystallographic value (pm)	XANES fit values (pm)
fcc Cu	Cu–Cu	256	Cu reference foil: 264 Reduced catalyst: 264
Monoclinic CuO	Cu–O	195–196	CuO reference: 201–202 Oxidized catalyst: 210–211

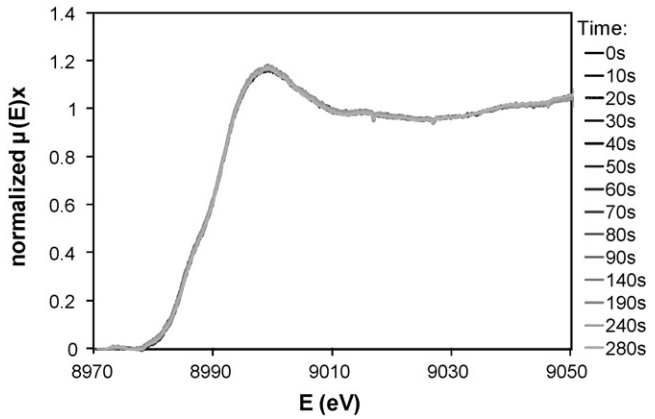

Fig. 10. Evolution of Cu K XANES spectra of $CuO–CeO_2/Al_2O_3$ catalyst during total oxidation reaction conditions ($1\%C_3H_8–5\%O_2$/He) at 723 K.

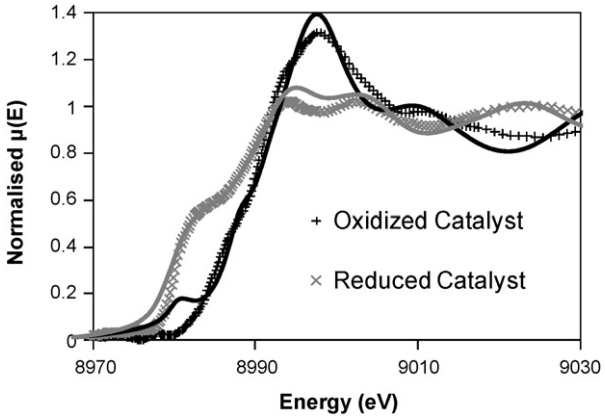

Fig. 11. Experimental Cu K XANES of the fully oxidized (+) and fully reduced (×) catalyst together with the respective theoretical fit (full lines, calculated with the structural parameters given in Table 3).

conditions as determined from the LCF analysis, i.e. 70 kJ/mol. To explain this finding, the following rationale can be envisaged. It is commonly proposed that the total oxidation reaction over a metal oxide catalyst proceeds via a Mars–van-Krevelen scheme [36]. The first step in the Mars–van-Krevelen reaction scheme is the reduction of the catalyst surface by the adsorbed organic compound. After the oxidized organic compound desorbs from the surface, in the final step, the reduced catalyst is re-oxidized by gas phase oxygen. Similar to the reaction scheme proposed by Martínez-Arias et al. [37,38] for the oxidation of CO with O_2 over a $CuO–CeO_2$ catalyst, propane total oxidation over the $CuO–CeO_2/Al_2O_3$ catalyst can be thought to proceed via a redox mechanism that involves the reduction of CuO to Cu_2O by C_3H_8, followed by the re-oxidation of Cu_2O to CuO by molecular oxygen. Since the activation energy for propane total oxidation is equal to the activation energy of catalyst reduction while catalyst oxidation requires a lower activation energy, these results point to a Mars–van-Krevelen reaction scheme with the copper phase of the catalyst being close to a fully oxidized state.

This assumption is also supported by the XANES analysis (see Fig. 10). No changes are observed in the Cu K XANES spectra of the $CuO–CeO_2/Al_2O_3$ catalyst during total oxidation conditions, indicating that the copper phase remains fully oxidized under total oxidation conditions. Therefore, when feeding a gas mixture of C_3H_8 and O_2 with a molar ratio of 1:5 (i.e. a stoichiometric ratio for the total oxidation reaction), the catalyst composition does not change on the time scale of reaction. Although oxygen is removed from the active phase of the catalyst for oxidizing the hydrocarbon, the oxygen vacancies are replenished so quickly by the oxygen present in the reactant mixture that the catalyst maintains a steady Cu^{2+} state.

3.5. Structural insights based on theoretical calculations

In order to clarify the short range order of the structure of the active phase before and after the treatment of the catalyst with propane and to obtain bond distances between neighboring atoms, theoretical spectra were fitted to corresponding experimental spectra using FDMNES. The experimental and calculated Cu K XANES spectra of the reduced and oxidized catalyst are shown in Fig. 11 and the resulting bond distances are summarized in Table 4.

From the theoretical fit on the experimental data, no difference was found between the fully reduced catalyst and the Cu foil. On the other hand, the fully oxidized catalyst has a CuO-like structure with elongated Cu–O bonds. As seen from the summarized results in Table 2, the Cu–Cu bond distance of the catalyst under reduction conditions is the same as the one in a Cu reference foil, i.e. 264 pm. However, the oxidized catalyst has significantly larger Cu–O bond distances (210–211 pm) than the CuO reference sample (201–202 pm). This result indicates that the Cu–O bond is weaker in the oxidized catalyst compared to the unsupported CuO reference, suggesting that removal of oxygen from the copper phase is easier during catalyst reduction and in total oxidation reaction conditions. This lengthening and weakening of the Cu–O bond has also been confirmed in the Cu doped CeO_2 system using density functional theory and it was held responsible for the lower reduction temperature of the CuO phase in a $CuO–CeO_2$ catalyst during H_2-TPR [39,40].

4. Conclusions

The structure and activity of a $CuO–CeO_2/Al_2O_3$ catalyst have been studied under reduction, oxidation and total oxidation reaction conditions by time-resolved *operando* Cu K XANES measurements combined with mass spectrometry. The copper phase remains fully oxidized under total oxidation reaction conditions. Three Cu species, i.e. Cu^{2+}, Cu^{1+} and Cu^0 are present during catalyst reduction and re-oxidation cycles evidencing the occurrence of a two-step mechanism. A similar activation energy of 70 kJ/mol is obtained for reduction of the catalyst with propane and for total oxidation of propane. On the other hand, catalyst re-oxidation occurs faster and has a lower activation energy, i.e. 24 kJ/mol, than its reduction. This points to a Mars–van-Krevelen reaction scheme with the copper phase of the catalyst being close to a fully oxidized state. In addition, ab initio calculated spectra allow to describe the experimental XANES of the $CuO–CeO_2/Al_2O_3$ catalyst. The local

structure of copper in the reduced catalyst is well in accordance with that of the metallic copper. However, the oxidized catalyst has weakened Cu–O bonds, thus making removal of oxygen from the catalyst easier as compared to an unsupported CuO phase, which can explain its enhanced activity in the total oxidation of propane.

Acknowledgements

The authors acknowledge ESRF for provision of synchrotron radiation facilities, IDECAT and GOA for financial support, and thank Dr. Mark Newton of the ID24 beamline for his support during the experiments.

References

[1] B. Solsona, I. Vázquez, T. Garcia, T.E. Davies, S.H. Taylor, Catal. Lett. 116 (2007) 116.
[2] I. Yuranov, N. Dunand, L. Kiwi-Minsker, A. Renken, Appl. Catal. B 36 (2002) 183.
[3] E.M. Cordi, J.L. Falconer, J. Catal. 162 (1996) 104.
[4] T. Mitsui, K. Tsutsui, T. Matsui, R. Kikuchi, K. Eguchi, Appl. Catal. B 81 (2008) 56.
[5] W.B. Li, J.X. Wang, H. Gong, Catal. Today 148 (2009) 81.
[6] H. Einaga, S. Futamura, React. Kinet. Catal. Lett. 81 (2004) 121.
[7] M. Turco, C. Cammarano, G. Bagnasco, E. Moretti, L. Storaro, A. Talon, M. Lenarda, Appl. Catal. B 91 (2009) 101.
[8] J. Papavasiliou, G. Avgouropoulos, T. Ioannides, Appl. Catal. B 69 (2007) 226.
[9] Y. Liu, T. Hayakawa, K. Suzuki, S. Hamakawa, T. Tsunoda, T. Ishii, M. Kumagai, Appl. Catal. A 223 (2002) 137.
[10] O. Ilinich, W. Ruettinger, X. Liu, R. Farrauto, J. Catal. 247 (2007) 112.
[11] X. Wang, J.A. Rodriguez, J.C. Hanson, D. Gamarra, A. Martínez-Arias, M. Fernández-García, J. Phys. Chem. B 110 (2006) 428.
[12] P.-O. Larsson, A. Andersson, Appl. Catal. B 24 (2000) 175.
[13] P.-O. Larsson, A. Andersson, J. Catal. 179 (1998) 72.
[14] M. Fernández-García, E. Gómez- Rebollo, A. Guerrero-Ruiz, J.C. Conesa, J. Soria, J. Catal. 172 (1997) 146.
[15] M. Ferrandon, B. Ferrand, E. Björnbom, F. Klingstedt, A. Kalantar Neyestanaki, H. Karhu, I.J. Väyrynen, J. Catal. 202 (2001) 354.
[16] P. Bera, S. Mitra, S. Sampath, M.S. Hegde, Chem. Commun. (2001) 927.
[17] G. Silversmit, H. Poelman, V. Balcaen, P.M. Heynderickx, M. Olea, S. Nikitenko, W. Bras, P.F. Smet, D. Poelman, R. De Gryse, M.-F. Reniers, G.B. Marin, J. Phys. Chem. Solids 70 (2009) 1274.
[18] J.-C. Labiche, O. Mathon, S. Pascarelli, M.A. Newton, G. Guilera Ferre, C. Curfs, G. Vaughan, A. Homs, D. Fernandez Carreiras, Rev. Sci. Instrum. 78 (2007) 091301.
[19] J.-D. Grunwaldt, A.M. Molenbroek, N.-Y. Topsøe, H. Topsøe, B.S. Clausen, J. Catal. 194 (2000) 452.
[20] M.A. Newton, F.G. Fiddy, G. Guilera, B. Jyoti, J. Evans, Chem. Commun. (2005) 118.
[21] B. Ravel, M. Newville, J. Synchrotron Radiat. 12 (2005) 537.
[22] J.-D. Grunwaldt, M. Caravati, S. Hannemann, A. Baiker, Phys. Chem. Chem. Phys. 6 (2004) 3037.
[23] T. Ressler, J. Wienold, R.E. Jentoft, T. Neisius, M.M. Günter, Top. Catal. 18 (2002) 45.
[24] Y. Joly, Phys. Rev. B 63 (2001) 125120.
[25] C. Prestipino, G. Berlier, F.X.L.I. Xamena, G. Spoto, S. Bordiga, A. Zecchina, G.T. Palomino, T. Yamamoto, C. Lamberti, Chem. Phys. Lett. 363 (2002) 389.
[26] L.-S. Kau, D.J. Spira-Solomon, J.E. Penner-Hahn, K.O. Hodgson, E.I. Solomon, J. Am. Chem. Soc. 109 (1987) 6433.
[27] A. Martínez-Arias, R. Cataluña, J.C. Conesa, J. Soria, J. Phys. Chem. B 102 (1998) 809.
[28] M.M. Gunter, T. Ressler, R.E. Jenotoft, B. Bems, J. Catal. 203 (2001) 133.
[29] T.L. Reitz, P.L. Lee, K.F. Czaplewski, J.C. Lang, K.E. Popp, H.H. Kung, J. Catal. 199 (2001) 193.
[30] A. Caballero, J.J. Morales, A.M. Cordon, J.P. Holgado, J.P. Espinos, A.R. Gonzalez-Elipe, J. Catal. 235 (2005) 295.
[31] R. Bulánek, B. Wichterlová, Z. Sobalík, J. Yichỳ, Appl. Catal. B 31 (2001) 13.
[32] N.B. Castagnola, A.J. Kropf, C.L. Marshall, Appl. Catal. A 290 (2005) 110.
[33] J.Y. Kim, J.A. Rodriguez, J.C. Hanson, A.I. Frenkel, P.L. Lee, J. Am. Chem. Soc. 125 (2003) 10684.
[34] J.A. Rodriguez, J.Y. Kim, J.C. Hanson, M. Pérez, A.I. Frenkel, Catal. Lett. 85 (2003) 247.
[35] D. Klvana, J. Vaillancourt, J. Kirchnerova, J. Chaouki, Appl. Catal. A 109 (1994) 181.
[36] M.A. Vannice, Catal. Today 123 (2007) 18.
[37] A. Martínez-Arias, M. Fernández-García, O. Gálvez, J.M. Coronado, J.A. Anderson, J.C. Conesa, J. Soria, G. Munuera, J. Catal. 195 (2000) 207.
[38] A. Martínez-Arias, A.B. Hungría, M. Fernández-García, J.A. Anderson, J.C. Conesa, J. Soria, G. Munuera, J. Phys. Chem. B 108 (2004) 17983.
[39] V. Shapovalov, H. Metiu, J. Catal. 245 (2007) 205.
[40] J.-Y. Luo, M. Meng, Y.-Q. Zha, L.-H. Guo, J. Phys. Chem. C 112 (2008) 8694.